Bulletin of Engineering Geology and the Environment (2023) 82:52
https://doi.org/10.1007/s10064-023-03067-w

ORIGINAL PAPER

Stability charts for undrained clay slopes considering soil anisotropic characteristics

Yongqin Li[2] · ATC Goh[4] · Runhong Zhang[2] · Wengang Zhang[1,2,3]

Received: 18 November 2021 / Accepted: 1 January 2023 / Published online: 19 January 2023

Abstract
It is generally recognized that the stress-induced anisotropy of undrained cohesive soil has a significant influence on the factor of safety of slopes. In this study, a simplified method is proposed to evaluate the slope stability considering soil anisotropic shear strength. An advanced constitutive model is used to characterize the anisotropic behavior of strength and stiffness of cohesive soil caused by the rotation of principal stress direction. A series of finite element analysis is carried out using the strength reduction method to calculate the safety factor of the undrained clay slope. The stability chart developed by Taylor (1937) has been adapted to take into consideration the anisotropic conditions of the clay slope. The stability number and failure modes of undrained clay slopes with different geometries and depths to hard stratum can be quickly assessed using the proposed design charts. Additionally, the feasibility of replacing complex anisotropy analysis with average isotropic constant undrained strength is discussed. Different suggestions are proposed for gentle and steep slopes. Findings of the present study can be a helpful supplement to the existing slope stability assessment for unreinforced undrained clay slopes.

Keywords Finite element analysis · Undrained clay slope · Stability chart · Stress-induced anisotropy

Introduction

Landslide caused by slope failure has become one of the major geological disasters all over the world. The management of unfavorable geological slope has been one of the key scientific issues in the construction and operation of infrastructure in China. Slope safety evaluation is a significant prerequisite for geotechnical decision-making in landslide disaster prevention. The deterministic analysis with the factor of safety (FS) is still the most frequently employed method to evaluate the stability of the natural and engineered slopes (Chen et al. 2020a, b, c; Gao et al. 2019). At present, the most convenient method for calculating the slope safety of factor is the empirical chart method, and the numerical tools are widely employed to distinguish and visualize the failure modes of slopes under different conditions. Whatever method is adopted, it is necessary to consider the realistic properties and state of the slope soil comprehensively in order to obtain reliable results.

Due to the existence of lateral free surface and the unloading effect in slope, the stress redistribution is encountered of necessity. The stress state of soil body at different positions of slope is significantly discrepant, and the orientation of principal stress suffers various degrees of rotation (Fig. 1). The mechanical characteristic of soil which changed due to the varied stress states is termed the stress-induced anisotropy (Hu et al 2020; Li et al. 2021; Zhang et al. 2020; Li and Zhang 2020). Worldwide specialties have proposed many new constitutive models which are capable of featuring this soil anisotropic behavior for both granular and cohesive soil (Cudny and Staszewska 2021; Ghorbani and Alrey 2021; Ghorbani et al. 2021). Influenced by the stress-induced anisotropy, the dominant properties which have great impact on soil engineering behavior include the strength and stiffness (Hwang et al. 2002; Xu et al. 2021). Liu et al. (2021) investigated the qualitative relationships between principal stress directions and the anisotropic behavior, i.e.,

✉ Wengang Zhang
zhangwg@cqu.edu.cn

[1] Key Laboratory of New Technology for Construction of Cities in Mountain Area, Chongqing University, Chongqing, China

[2] School of Civil Engineering, Chongqing University, Chongqing, China

[3] National Joint Engineering Research Center of Geohazards Prevention in the Reservoir Areas, Chongqing University, Chongqing, China

[4] School of Civil and Environmental Engineering, Nanyang Technological University, Singapore, Singapore

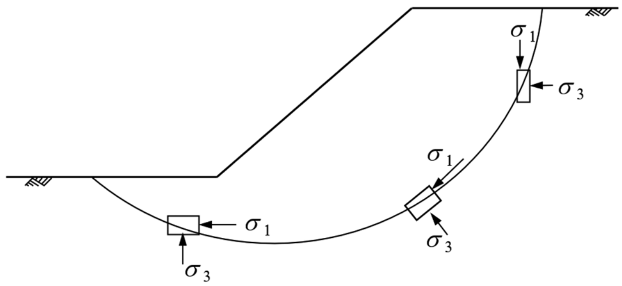

Fig. 1 Principal stress orientation variation in excavated slope

stress–strain development, after principal stress axis cycling. They concluded that the normalized strength of the remodeled loess nonlinearly decreases as the principal stress angle enlarges and reaches its lowest value when the principal stress angle is 90°. They further proposed the equations for calculating the anisotropic strength of loess under general stress condition. Zapata-Medina et al. (2020) evaluated the stiffness and strength anisotropy of some clay specimen from certain regions through a series of tests. They point out that for most overconsolidated clays, the stiffness anisotropy degree increases with the over consolidation ratio (OCR). And the failure friction angle under triaxial extension test is slightly larger than that under compression failure mode according to the effective stress failure envelopes.

With feasible description of soil stress-induced anisotropy, a train of research has introduced this feature into the analysis of slope stability (Conesa et al. 2019; Rao et al. 2019; Stockton et al 2019; Tang et al 2020; Ning et al 2021; Yeh et al. 2020). Liu et al. (2018) proposed the expressions of shear strength parameters by incorporating an anisotropic state scalar index, and applied it to slope stability analysis. According to their calculation, the factor of safety can be reduced by 22.0% when considering the anisotropy of strength. Rao et al. (2019) conducted a three-dimensional upper-bound limit analysis on reinforced slope stability problem and reached the conclusion that the factor of safety is negatively correlated with the anisotropic degree. Xia and Chen (2018) addressing at the seismic stability problem of an anchored slope analyzed the effect of anisotropic shear strength parameters. When the anisotropy is becoming notable, the yield acceleration factor showed obvious decreasing trend, indicating the slope seismic stability continuously reducing. The similar conclusions of the above studies indicate the importance of considering soil anisotropy in accurately evaluating the slope stability.

In this paper, a well-known empirical chart of assessing the slope factor of safety is firstly reviewed. Then, the quantification of clay strength and stiffness anisotropy is included through introducing the advanced constitutive model. The stability of unreinforced slope is investigated adopting the strength reduction method. A series of finite element models with different slope geometries and soil properties are established, and the numerical results are organized and analyzed to update the empirical chart.

Evolution of Taylor's chart

Currently, empirical charts are used in practical cases as handy and efficient means for evaluating slope stability (Chen et al.2020a, b, c). Many stability charts with no requirement of tedious calculation are constructed and improved. The line-based stability charts for slopes raises great convenience in rapidly assessing FOS (Lim et al. 2016; Sahoo et al. 2019, 2020; Liu et al. 2022). Various forms of line-based stability charts are in use. Among existing slope stability charts, Taylor (1937) once used the friction circle method to propose simple design charts to assess the slope stability. The charts established determined relations to correlate the slope stability number with slope geometry, including slope angle and relative slope height. The charts were designed targeting at the homogeneous undrained clay slope stability problems, in which the ϕ_u=0. Three modes of failure circles were demarcated in Taylor (1937), namely shallow toe circle, deep toe circle, and mid-point circle, which will be introduced in the "Slip circle modes" section.

Based on Taylor's achievements, Baker (2003) made an advancement of Taylor's stability problem with quantization of two-dimensional coordinate system to capture the slip circle configurations within the slope plane. Steward et al. (2011) made further improvement in which compound slip circle modes were proposed considering the heterogeneous site soil condition. Five more specific failure modes were proposed taking the underlying hard soil layer into account, which is of more significance for practical engineering.

Stability number

In addition to the traditional safety factor index to represent the stability of slopes, a new dimensionless stability number N_s linked with soil physical and mechanical properties and slope geometry was proposed:

$$N_s = \frac{\gamma H}{s_{u,\mathrm{mob}}} = \frac{\gamma HF}{s_u} \tag{1}$$

where γ is the unit weight of the undrained clayey soil, H represents the slope height, $s_{u,\mathrm{mob}}$ is the undrained shear strength mobilized along the slip circle within the clayey soil, while s_u stands for the undrained shear strength of the clayey soil, and F is the factor of safety calculated through strength reduction method. By normalizing the factor of safety, the stability number can be used to compare the slope stability conditions under different slope shapes and soil strengths.

Slip circle modes

For undrained homogeneous clay slope, three types of slope failure modes were identified according to a traditional cylindrical critical slip surface that is not astricted by deep buried hard stratum. The slip circle conditions are namely shallow toe circle, deep toe circle, and base circle as shown in Fig. 2. It was point out that for some steep slopes, the failure surface is generated above the slope toe elevation along a circular arc which is passing through the slope toe (as Fig. 2a shows the shallow toe circle mode). When the slope gradually becomes gentle, the sliding surface may break through the bottom of the slope and continue to develop downward, but still cut out from the toe, this failure mode is called deep toe circle. Furthermore, without the existence of deep stiff soil layer, the sliding surface in soft clay may continue to extend, the critical failure surface reaches the area beneath the slope toe, which leads to the base circle failure mode. The volume of the sliding body increases significantly as the slip circle mode changes.

The burial depth of stiff stratum plays dominant role in the stability and potential failure mode of multi-layered soil slope. The burial depth of stiff stratum is characterized with the index n_d as shown in Fig. 3; it is the ratio of the distance from the top of the slope to the hard soil layer over the slope height. In view of the slope angle, buried depth of hard soil and soil strength, Steward et al. (2011) identified the slip surface of clay slope into five types as shown in Fig. 3.

Taylor's chart for undrained clay slopes

A typical form of Taylor's chart is shown in Fig. 4. The slope stability number can be obtained according to the general slope shape information with reference to the chart. Then the factor of safety can be calculated according to the N_S equations (Eq. 1) with knowledge of soil properties.

The improved charts proposed by Steward et al. (2011) use similar form and principles, only the division of slip circle modes is different. Therefore, the work of Steward et al. (2011) is not described in detail here.

Currently, the existed stability charts are generally designed for isotropic clay slope; the complex clay behavior is not taken into account. In this study, the difference in soil rotational principal stress is considered to capture the differential behavior of soil under various stress paths. The objective of this paper is to update the stability charts for clay slope with underlying hard soil with special focus on the clay stress-induced anisotropic behavior. To some extent, it can provide a useful reference to supplement and complete previous stability charts.

Soil anisotropic model

The importance and necessity of considering stress-induced anisotropy for the analysis of slope stability problems have been discussed in several studies (Stockton et al 2019; Tang and Wei 2019; Ning et al 2021). In this study, the NGI-ADP anisotropic constitutive model has been adopted. The core of this model is the ADP concept proposed by Bjerrum (1973). The model defines the behavior of clay under any stress state through three characteristic stress–strain relations under three different laboratory test paths: triaxial extension, direct simple shear, and triaxial compression. The three shear states are represented by the active (A), direct simple shear (DSS), and passive (P) loading stress paths, which form the kernel of the ADP concept. The model uses the undrained shear strengths under the three stress paths to define the anisotropic strength, which are $s_u{}^A$, $s_u{}^{DSS}$, and $s_u{}^P$, respectively.

In order to model the stiffness anisotropy, the model employs three shear strains at failure, γ_f^C for triaxial compression, γ_f^{DSS} for direct simple shear, and γ_f^E for triaxial extension. Combined with the undrained shear strength of the corresponding stress path, the anisotropic stiffness under

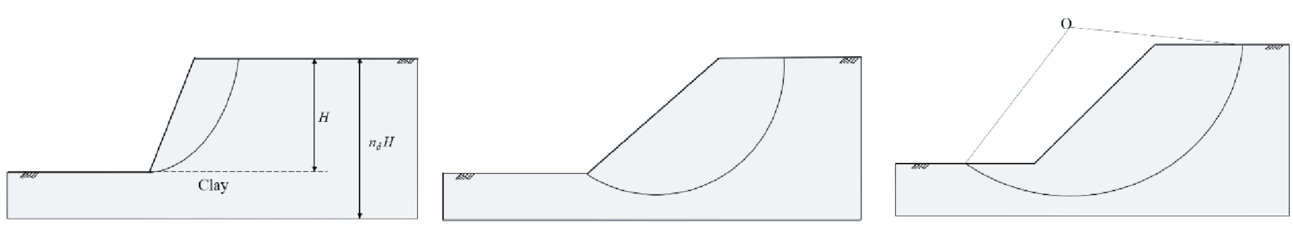

(a) Shallow toe circle **(b)** deep toe circle **(c)** base circle

Fig. 2 Failure modes in Taylor (1937)

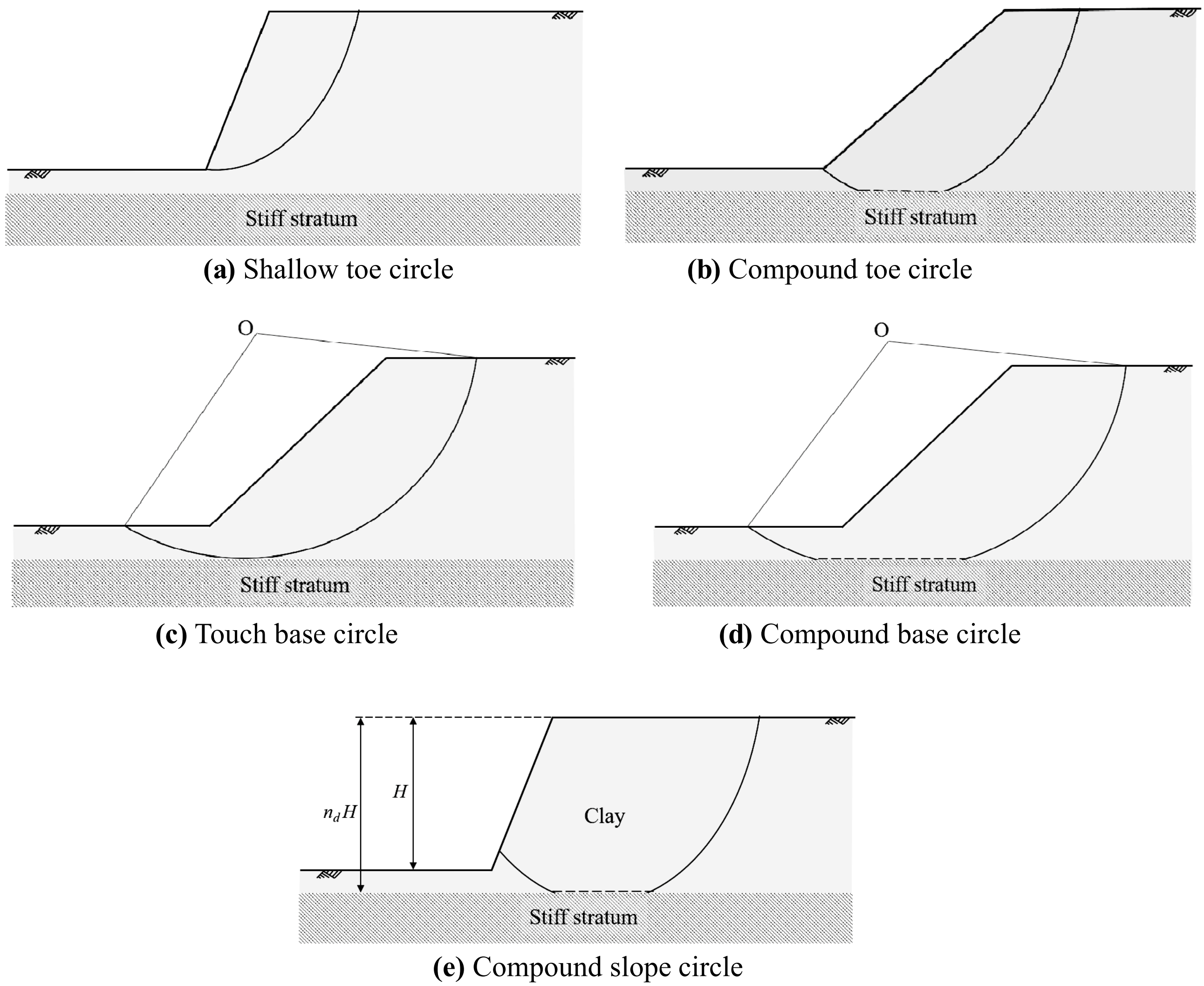

Fig. 3 Compound failure modes for multi-layered slope (Steward et al. 2011)

the discrepant loading paths can be obtained. In addition to these three stress conditions, the model implements elliptical interpolation between failure strain and strength for arbitrary stress paths.

The shear modulus G_{ur} for both loading and unloading is assumed to be isotropic and stress-independent when the soil is elastic. The development of shear stress and strain in the plastic state under the three paths is shown in Fig. 5. The yield criterion for the model is constructed based on a translated approximated Tresca criterion. In plane strain condition, it can be represented as

$$f = \sqrt{\left(\frac{\sigma_{yy} - \sigma_{xx}}{2} - (1-k)\tau_0 - k\frac{s_u^A - s_u^P}{2}\right)^2 + \left(\tau_{xy}\frac{s_u^A + s_u^P}{2s_u^{DSS}}\right)^2} - k\frac{s_u^A + s_u^P}{2} = 0 \quad (2)$$

where $k = 2\frac{\sqrt{\gamma^p/\gamma_f^p}}{1+\gamma^p/\gamma_f^p}$ when $\gamma^p < \gamma_f^p$, in which γ^p, γ_f^p are the plastic shear strain and the failure plastic shear strain; otherwise, $k = 1$.

Other than the six key input parameters described above, the other pre-defined input parameters required in the constitutive model are listed in Table 1. Note that the units for some indices are expressed under the plane strain state. The unloading/reloading shear modulus in the elastic stage is characterized by the dimensionless ratio G_{ur} divided by the active undrained shear strength.

In this model, the s_u shear strength ratio s_u^P/s_u^A is the critical parameter that directly characterizes the strength anisotropy. The ratio ranges from 0 to 1. The s_u ratio of 1 represents the ideal isotropic condition. The s_u^{DSS}/s_u^A is correlated with the s_u^P/s_u^A in this model and is defined to be

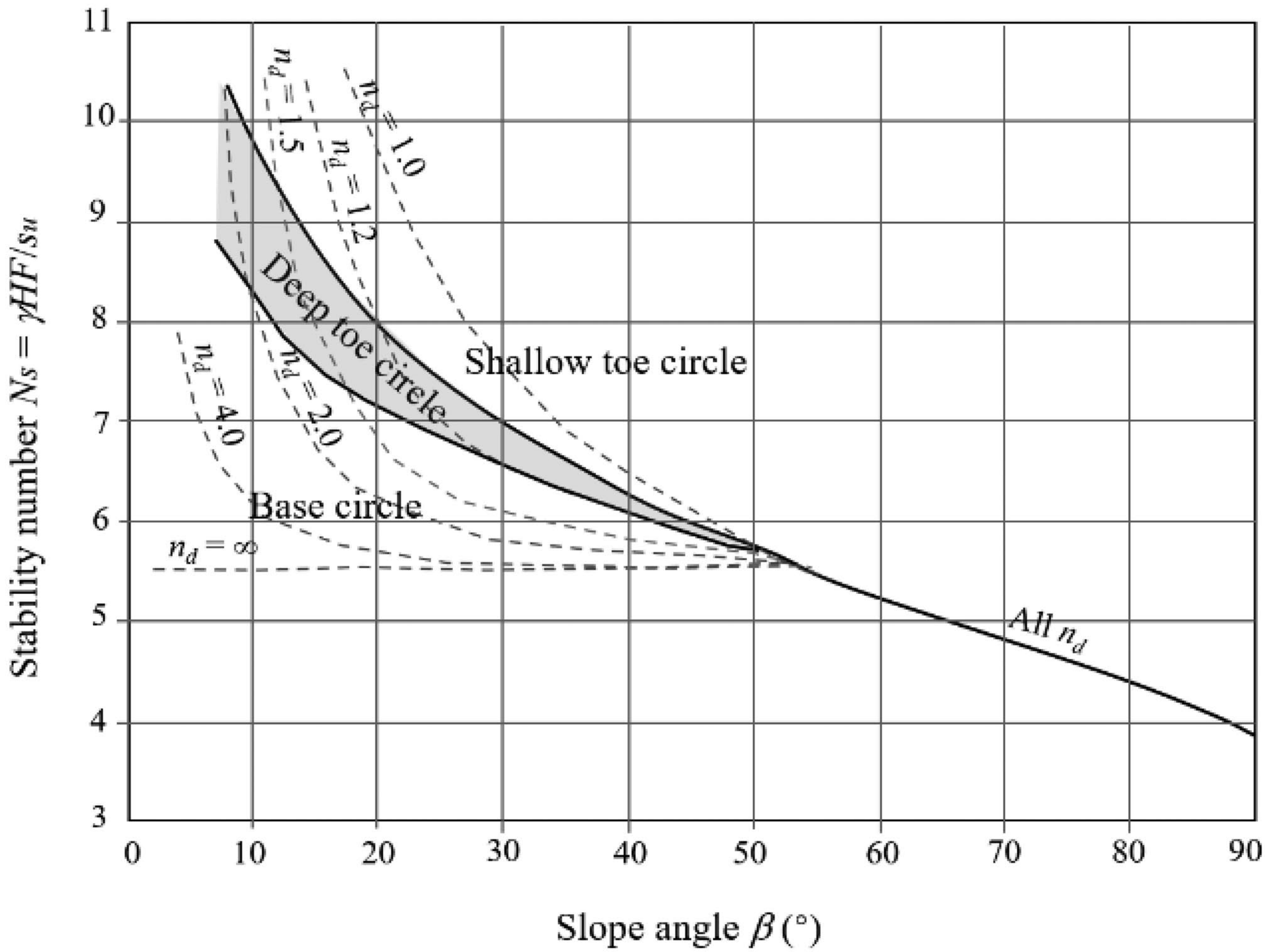

Fig. 4 Typical form of Taylor's chart

$$\frac{s_u^{DSS}}{s_u^A} = (1 + \frac{s_u^P}{s_u^A})/2 \tag{3}$$

This model NGI-ADP has been successfully employed in analyzing braced excavation displacement (Zhang et al. 2020) and embankment stability (Verreydt et al. 2019). It was further improved to describe the strain-softening behavior (Jostad 2014; Huynh et al. 2019), named NGI-ADPSoft. The model was implemented into a finite element procedure to perform simulations according to a full-scale failure test on soft clay deposit. It showed satisfactory capacity in predicting failure loads, confirming its feasibility in simulating clay post-peak softening behavior (D'Ignazio et al. 2017). However, the anisotropic characteristic in undrained strength and stiffness stands the key focus of this study; the perfect plasticity is employed as Fig. 5 indicates; no softening analysis is included in the following content.

Slope stability analysis

Finite element model

In this study, the anisotropic clay slopes were analyzed using the finite element software Plaxis (Panagoulias et al. 2018). A typical cross-section of the slope is shown in Fig. 6. The total thickness of the soft clay is 40 m. The slope height H is 10 m, and the depth from the toe of the slope to the underlying hard stratum/bedrock H_D is 30 m. In subsequent parametric studies, H_D is decreased to study the effects of the hard stratum on the stability analysis. Only the soft clay is modeled with the underlying bedrock represented by the bottom boundary of the FE model. The left and right boundaries of the finite element model are assumed to be fixed horizontally but free to move vertically, while the bottom boundary is assumed to be fixed both horizontally and

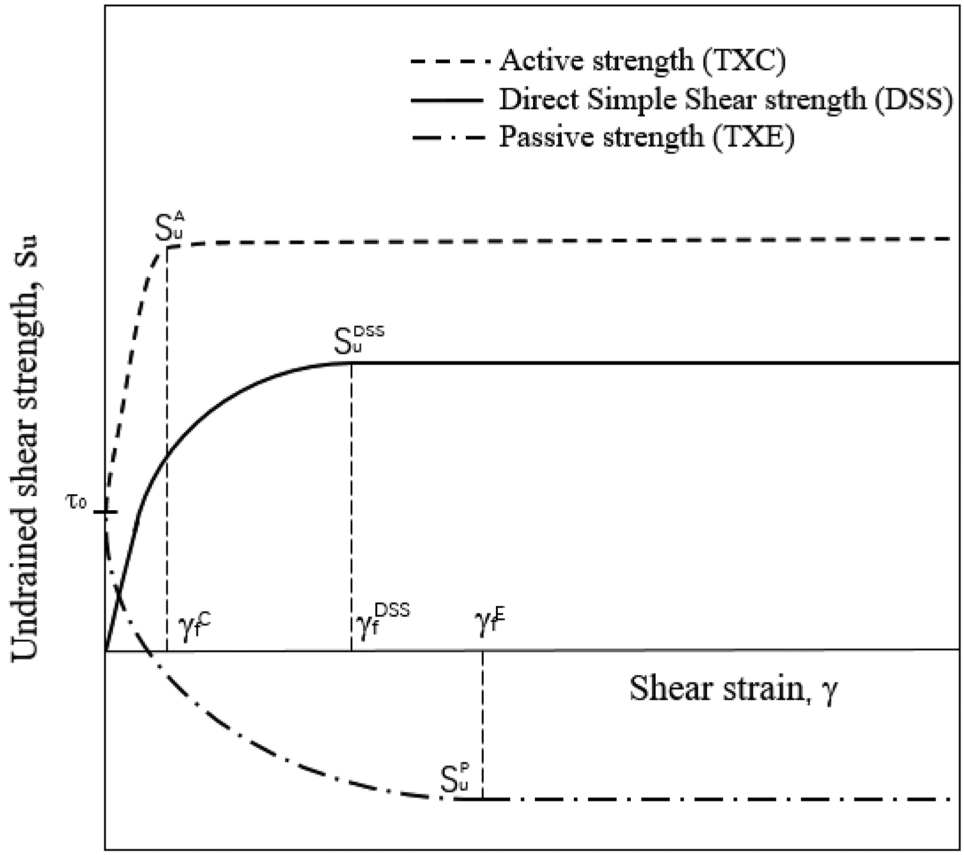

Fig. 5 Stress–strain curves for three stress paths adopted in NGI-ADP model

vertically. The left and right vertical boundaries are located sufficiently away from the slope so as to have no influence on the slope response.

The properties of the soft clay are shown in Table 2. For the simulation of slope excavation, total five excavation stages are included in which 2 m of soil is excavated. Table 3 shows the range of values of the parametric study. The range of the shear strength ratio s_u^P/s_u^A considered in this study is based on previous laboratory and in situ test findings from various researchers including Grimstad et al. (2012) and Ukritchon and Boonyatee (2015). Note that some related parameters vary correspondingly, such as y_{ref}.

A total of 180 cases are modeled and calculated in terms of different slope geometries and soil properties. The

Table 1 Input parameters of NGI-ADP model

Type	Parameter	Description	Unit (under plane strain state)
Strength	$s_{u,\mathrm{ref}}^A$	Reference (plane strain) active shear strength	kN/m^2/m
	y_{ref}	Reference depth	M
	$s_{u,inc}$	Increase of shear strength with depth	kN/m^2/m
	s_u^P/s_u^A	Ratio of (plain strain) passive shear strength over (plain strain) active shear strength	-
	s_u^{DSS}/s_u^A	Ratio of direct simple shear strength over (plain strain) active shear strength	-
Stiffness	G_u/s_u^A	Ratio unloading/reloading shear modulus over (plane strain) active shear strength	-
	γ_f^C	Shear strain at failure in triaxial compression	%
	γ_f^E	Shear strain at failure in triaxial extension	%
	γ_f^{DSS}	Shear strain at failure in direct simple shear	%
	υ	Poisson's ratio	-
Other	γ	Unit weight	kN/m^3

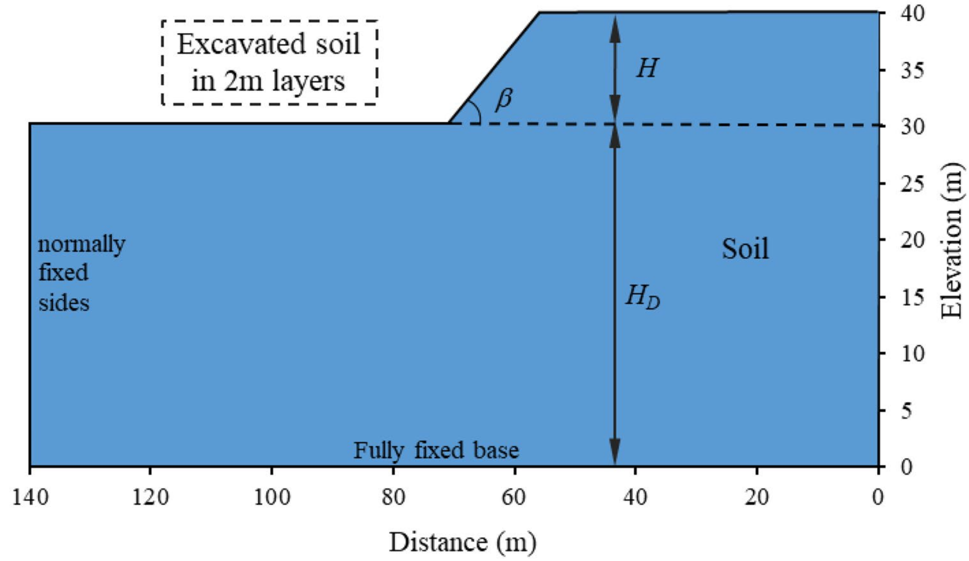

Fig. 6 Slope geometry with parameters

strength reduction method is adopted to determine the slope stability, as its feasibility is verified by abundant researches (Yuan et al. 2020; Tu et al. 2016). The method is designed to reduce the material properties, normally the strength indices. When the stress of an element exceeds the yield surface, the stress it cannot hold gradually transfers to surrounding soil element until a continuous sliding surface is formed. The reduction factor at the failure situation is the safety factor of the slope.

A total of 4164 triangular elements with 15 nodes were included. The default 15-node triangle element type provides fourth-order interpolation for displacement and is more accurate for strength reduction calculation in contrast with 6-node element. No structural members were included in the numerical model. The efforts of numerical model modification, repeated calculation, and result output can be completed by the interactive code of Plaxis and Python, which greatly improves the efficiency of modeling and post-processing. The modification, calculation, and extraction of a single FE model can be approximately completed in 2 min. The calculated results including development of slope stability number, soil displacement field, and sliding surface mode are extracted and analyzed.

Results analysis

Slope stability

In this study, the stability number N_s described in Eq. (1) is used to assess the stability of the slope. For anisotropic soils, the s_u term in Eq. (1) is replaced by s_u^A. The factor of safety is determined from the finite element analysis using the strength reduction method. The stability number enables slopes with different geometries and soil properties to be compared with a higher N_s denoting a higher factor of safety.

Figure 7 shows the influence of the shear strength ratio s_u and the slope angle on the stability number. The general trend is for the stability number to decrease as the slope angle increases and the shear strength ratio decreases. When the shear strength ratio = 0.5, the stability number decreases by about 1/3 compared with the isotropic clay with shear strength ratio = 1.0 for very gentle slopes. As the slope angle increases, the stability number generally converges irrespective of the shear strength ratio. For steep slopes, the

Table 2 Properties of anisotropic soft clay

NGI-ADP soil model (undrained C)			
γ (kN/m^3)	16	$s_u^{C,TX}/s_u^A$	0.99
G_u/s_u^A	600	y_{ref} (m)	20
γ_f^C (%)	0.75	$s_{u,\text{inc}}$ (kPa/m)	0
γ_f^E (%)	3.5	s_u^P/s_u^A	1.0
γ_f^{DSS} (%)	1.735	τ_0/s_u^A	0.7
$s_{u,\text{ref}}^A$ (kPa)	60	s_u^{DSS}/s_u^A	$=(1+s_u^P/s_u^A)/2$
Poisson's ratio υ_u	0.495		

Table 3 Variations of parameters for systematic analysis

Indices	Values
s_u^P/s_u^A	0.5, 0.6, 0.8, 1.0
Slope angle β (°)	10, 20, 30, 40, 50, 60, 70, 80, 90
Depth index n_d*	1, 1.5, 2, 3, 4

*$n_d(H+H_D)/H$

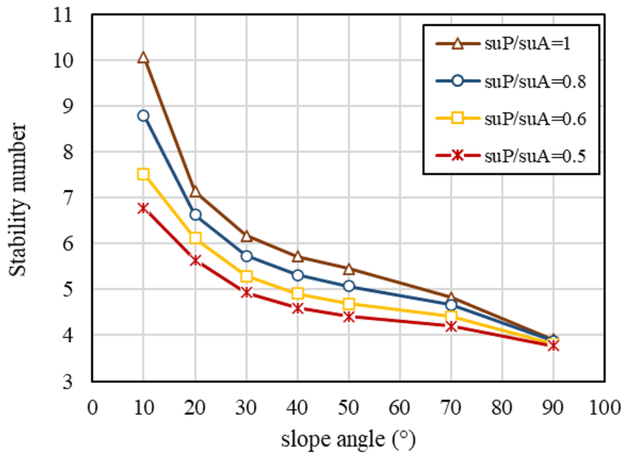

Fig. 7 Effects of slope angle and shear strength ratio on stability number

difference in the stability number is minimal. The results indicate that the clay anisotropy has a greater effect on the slope stability for a gentle slope compared with a steep slope. This is because for a steep slope, the failure mechanism is a shallow toe circle (Fig. 2a), and the stability is essentially governed by the active shear strength s_u^A. This is discussed further in the "Slope failure mechanism" section.

The influence of the depth of the hard stratum on the stability number is shown in Fig. 8. The lines indicate the different thickness of soft soil layer below the bottom level of slope with the solid lines representing the isotropic cases and the dotted lines representing the anisotropic cases for shear strength ratio = 0.5. As in Fig. 7, the results indicate that apart from the case of the vertical slope, the stability number for the anisotropic cases are lower than for the isotropic case. In addition, the results indicate that as the depth index n_d increases, the stability

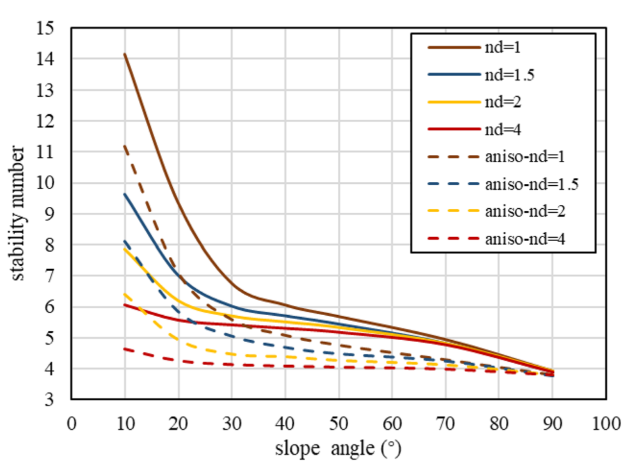

Fig. 8 Effects of depth to hard stratum on the stability number for $s_u^P/s_u^A = 0.5$ and 1.0

number reduces significantly for gentle slopes. When the slope angle β exceeds 60°, the differences become minimal. These phenomena are associated with the slope failure mechanisms, which will be discussed further in the "Slope failure mechanism" section.

Slope failure mechanism

As discussed in the "Slip circle modes" section, Steward et al. (2011) identified five different slip circle mechanisms: compound slope circle, compound toe circle, compound base circle, touch base circle, and shallow toe circle. As three of these circles are constrained by the hard stratum, the failure mechanism comprises of two separated arcs and a straight line along the soil-hard stratum interface as shown in Fig. 9b, d, e. The remaining two failure slip circles as Fig. 9a, c are not affected by the hard stratum. The development of the five failure mechanisms for anisotropic soils ($s_u^P/s_u^A = 0.5$) in terms of total displacement contours is summarized as follows:

1. For steep slopes in which the slope angle $\beta > 60°$, the shape of the failure circle is a shallow toe circle (Fig. 2a) and is independent of the hard stratum. The displacement contours and vectors for a typical vertical slope are shown in Fig. 9a. The slip circle does not develop below the elevation of toe of the slope. The displacement vectors show significant lateral soil displacements and minimal deformation of the soil beneath the toe of the slope. Therefore, the depth index n_d which represents the relative depth to the hard stratum has minimal influence on the stability of steep slopes.
2. For a gentle slope with the hard stratum close to the bottom of the slope, the failure mechanism is a deep toe slip circle (as in Fig. 2b and Fig. 9b) that is cut off (i.e., intercepted) by the hard stratum and forms the compound toe circle.
3. For the base slip circle, the failure mechanism is either tangent to the hard stratum as or does not touch the hard stratum as shown in Fig. 9c. This generally occurs for gentle slopes where the hard stratum is quite deep.
4. For a gentle slope in which the depth to the hard stratum is small, the failure mechanism is a compound base circle (Fig. 9d).
5. The slope circle mechanism generally occurs in gentle slopes, with a deep slip surface as illustrated in Fig. 9c, d. However, when the depth to the hard stratum is very shallow, the compound slope circle mode is occasionally encountered as shown in Fig. 9e.

The plots in Fig. 9 indicate that the failure slip surfaces for isotropic soils and anisotropic soils are similar. However, they differ in terms of the magnitude of the slope

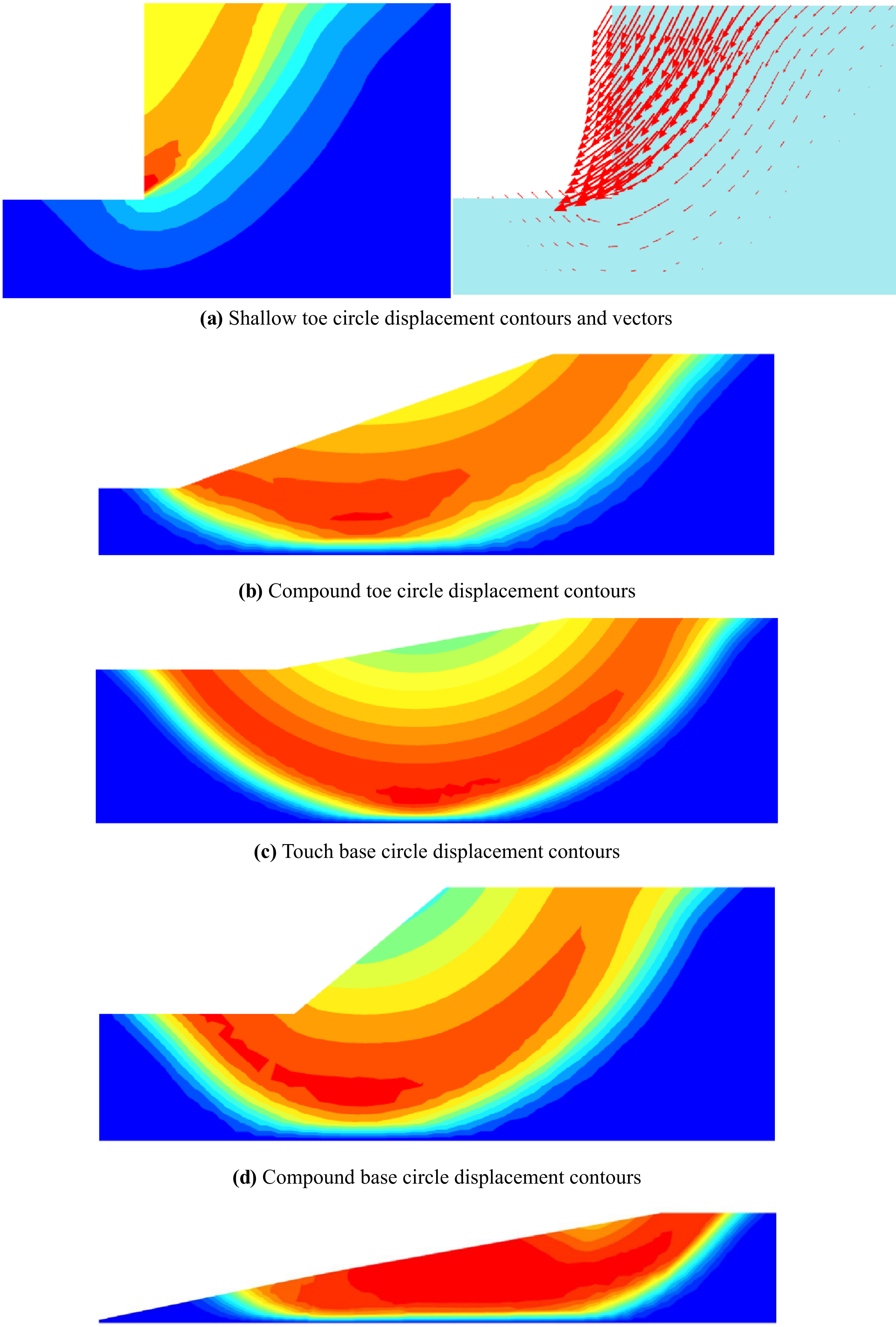

(a) Shallow toe circle displacement contours and vectors

(b) Compound toe circle displacement contours

(c) Touch base circle displacement contours

(d) Compound base circle displacement contours

(e) Compound slope circle displacement contours

Fig. 9 Deformation modes of slopes with various geometries displacements, the mobilized shear stress, and the factor of safety.

Average undrained shear strength

Because of the complexities involved in using a numerical approach to analyze a slope with anisotropic shear strength properties, this section explores the feasibility of using an "average" undrained shear strength to perform an equivalent isotropic stability analysis of the slope.

The average shear strength $s_{u,\mathrm{ave}}$ here is defined to be the average value of the active shear strength s_u^A and the passive shear strength s_u^P. For example, for the case with $s_u^P/s_u^A = 0.6$, the average shear strength $s_{u,\mathrm{ave}} = 0.8s_u^A$. A total of 70 isotropic analyses were carried out using $s_{u,\mathrm{ave}}$, and the computed factors of safety were compared with the corresponding anisotropic case. For all the cases, it was assumed that $n_d = 3$. The effects of substituting anisotropic degree with average strength are plotted in Fig. 10. The longitudinal coordinate represents the safety factor calculated using isotropic average shear strength verses the safety factor computed with anisotropic constitutive model. Table 4 lists some of the computed results for comparison.

The results indicate good agreement between the analyses using $s_{u,\mathrm{ave}}$ and the corresponding anisotropic cases for gentle slopes (i.e., slope angle is less than 60°), with relative errors of factor of safety of less than 5%. The performance of average isotropic constant undrained shear strength matches well with the anisotropic cases, indicating the approximate uniformity of the active and passive stress zones of soil mass. This phenomenon is consistent with the slope slip circle mode. For soft gentle slope with deep hard soil layer, the failure surface can be base circle, slope circle, or deep toe circle. The corresponding sliding angle is normally large, leading to extensive passive areas of soil.

While for steep slopes in which β exceeds 60°, the stability numbers of simplified average isotropic case are substantially smaller than the actual anisotropic results as marked in red in Table 4. The relative error reaches 18% for vertical slope. The lower stability number obtained using the average strength indicates that the average strength is obviously lower than the actual strength which is interpolated according to various stress state. Therefore, in the actual soil stress field, the soil under the active stress state accounts for the majority; the clay under passive stress covers less

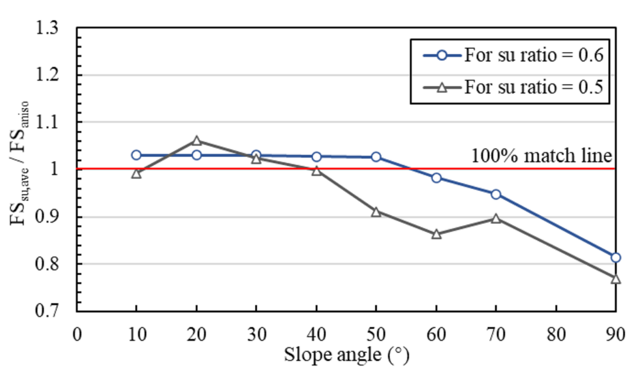

Fig. 10 The safety factor computed using average undrained shear strength

Table 4 Comparison of stability number using average strength and anisotropic cases

Slope angle (°)	n_d	Stability number		
		s_u^P/s_u^A=0.6	using $s_{u,ave}$	Relative error
10°	1.5	13.52	13.42	−0.76%
	2	10.69	10.75	0.54%
	3	8.45	8.71	3.05%
	4	7.74	7.97	2.99%
30°	1.5	8.44	8.24	−2.37%
	2	7.64	7.72	1.11%
	3	7.13	7.35	3.05%
	4	6.91	7.12	3.02%
50°	1.5	7.49	7.27	−2.97%
	2	7.13	7.18	0.69%
	3	6.88	7.06	2.71%
	4	6.77	7.02	3.74%
60°	1.5	7.10	6.44	−9.27%
	2	6.89	6.42	−6.84%
	3	6.74	6.40	−5.14%
	4	6.66	6.36	−4.47%
90°	1.5	6.30	5.22	−17.21%
	2	6.35	5.22	−17.77%
	3	6.33	5.16	−18.53%
	4	6.35	5.18	−18.47%

Table 5 Substitution effect of using "second-average" strength for steep slopes

Slope angle (°)	n_d	Stability number		
		s_u^P/s_u^A=0.6	Using $s_{u,ave}$'	Relative error
60°	1.5	7.10	7.68	8.17%
	2	6.89	7.08	2.76%
	3	6.74	6.945	3.04%
	4	6.66	6.9	3.60%
70	1.5	6.735	6.245	−7.28%
	2	6.5	6.22	−4.31%
	3	6.335	6.195	−2.21%
	4	6.27	5.97	−4.78%
90°	1.5	6.30	5.89	−6.51%
	2	6.35	5.95	−6.30%
	3	6.33	5.88	−7.11%
	4	6.35	5.98	−5.8 error

proportion as Fig. 9a shows. It was further discussed that for steep slopes, it is possible to use a larger "average" strength to substitute the complex anisotropic analysis. To this end, the "second-average" undrained shear strength $s_{u,\mathrm{ave}}' = (s_u^A + s_u^{DSS})/2$ is proposed. The effect of the simplified isotropic average undrained analysis for steep slopes is shown in Table 5.

It can be concluded that for clay slopes in which slope angle is less than 60°, the simplicity of using the average isotropic constant strength instead of anisotropic interpolation strength is feasible. However, for steep slopes, it is suggested that a larger and more reasonable substitution value, i.e. $s_{u,\mathrm{ave}}' = (s_u^A + s_u^{DSS})/2$, should be used to capture the practical slope response under stress-induced anisotropy.

Updated Taylor's chart

Stability chart for anisotropic undrained clay slope

As the feasibility of using simplified "average" strength index is validated, hundreds of calculations have been run to efficiently locate the diversions of different critical slip circle modes for anisotropic undrained clay slopes with various geometries. Relevant stability chart is updated based on Taylor's (1937) and Steward's (2011) work. The updated Taylor's chart is presented graphically in Fig. 11. The stability number is calculated using the undrained shear strength $s_{u,\mathrm{ave}} = (s_u^A + s_u^P)/2$ for gentle slopes, in which the slope angle β <60° .For steep slopes, the "second-average" strength $s_{u,\mathrm{ave}}' = (s_u^A + s_u^{DSS})/2$ is adopted. The *y*-axis represents the stability factor related to the safety factor, and the *x*-coordinate is the slope angle. The area enclosed by several groups of stiff stratum depth ratio (i.e., n_d) is divided into five sub-areas according to different sliding surface modes. In this study, five different slip circle modes were identified as the legend shows.

In Fig. 11, the blue area represents the failure mode of compound slope circle; it normally happens when the slope is gentle and the strata interface is very close to the bottom of the slope. The orange area covers the possibility of compound toe circle failure mode. When the depth of hard soil layer increases gradually, the green compound base circle mode becomes more possible. If the buried depth of hard soil is too deep to restrain the soft soil slope deformation, the touch base circle failure commonly occurs, which is marked in yellow. When the slope angle reaches 60°, it is very likely that the slope fails along the shallow toe circle. For very steep slopes, the sliding surface can hardly penetrate below the bottom elevation.

Fig. 11 Updated stability chart for anisotropic undrained clay slopes

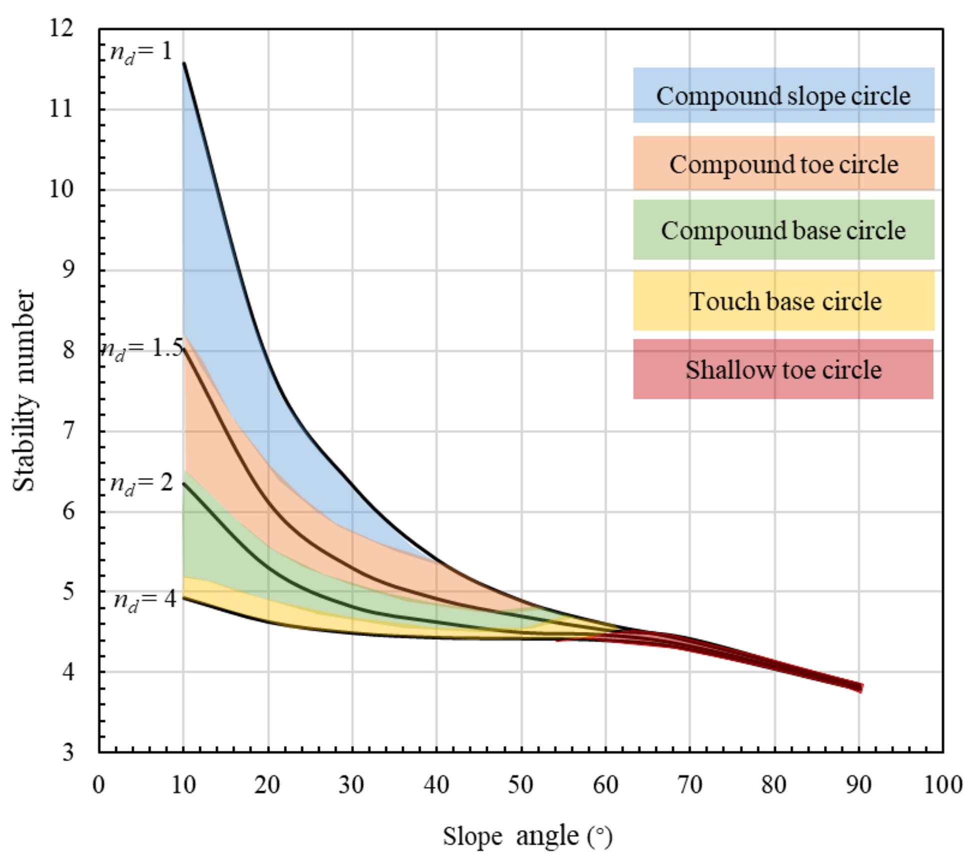

Case validations

Case 1

An undrained layered slope reported in Luo et al. (2019) was chosen. They employed the finite element tools to assess the slope failure pattern and safety factor of layered slope, which is available for validations of the presented anisotropic stability chart. For the two-layered slope in the referencing study, the average undrained shear strength of the upper clay is 25 kPa, unit weight $\gamma = 20\text{kN/m}^3$, and slope height $H = 5\text{m}$. The stability number can be read as 4.9 from figure n with $n_d = 2$ and $\beta = 26.5°$; the failure mode is identified to be compound base circle. From Eq. 1, the factor of safety can be calculated:

$$F = \frac{N_s \times s_{u,ave}}{\gamma H} = 1.22$$

In Luo et al. (2019), the safety factor calculated via finite element method is 1.27, and they identified the slip circle mode as compound type, which is very close to the results obtained from the presented stability chart.

Case 2

An example from a study (Tang and Wei 2019) which also considers the anisotropy of soil strength is employed as another validation. The model also established a homogeneous soil slope and simulated the underlying hard soil layer by limiting the displacement of the base boundary. In the referencing study, the effective stress strength indices were adopted, and they were converted into undrained shear strength according to correlation principles proposed by Cheng (2001). The slope information includes as follows: $s_{u,\text{ave}} = 146.9$ kPa, $\beta = 45°$, $n_\text{d} = 2$, $\gamma = 20\text{kN/m}^3$, $H = 20\text{m}$.

The stability number in view of n_d and β is $N_s = 4.6$, and the corresponding factor of safety is $F = 1.69$. The safety factor is quite similar to that of 1.78 calculated using the gravity increasing method in Tang and Wei (2019). However, there is no way to validate the correctness of slip circle mode because it is not mentioned in their study.

According to the identical results of the above two examples, it can be considered that the updated empirical chart performs well and can be used to estimate the stability and failure mode of anisotropic clay slopes with underlying stiff stratum.

Conclusions

The present study investigated the stability and possible sliding modes of the unreinforced slope with underlying stiff stratum and updated a well-known empirical chart by introducing the stress-induced anisotropy into slope stability analysis. A series of finite element models were established featuring with different slope geometries and soil properties, and the strength reduction method was employed to assess the slope stability. The main findings are as follows:

1. Through comparison of stability number between anisotropic and isotropic clay slopes, the slope stability may be overestimated ignoring the anisotropy characteristics of soil, especially for high and gentle slopes.
2. The burial depth of underlying stiff stratum plays a significant role in determining the slip circle mode. As the hard soil is buried deeper, the slope stability continuously decreases. While for steep slopes, stiff stratum has marginal effect on its stability number and failure mode.
3. The average isotropic constant undrained shear strength can be employed as the substitution for the stress-induced anisotropic strength and stiffness for gentle slopes. With the increase of slope angle, the effectiveness of substitution decreases gradually. Since the soil under passive stress state along the sliding surface is of minority for high and steep slopes, the actual overall strength is greater than the average shear strength. In this case, it is suggested to use a larger "second-average" strength to perform slope stability assessment.
4. A convenient empirical chart with consideration of clay strength and stiffness anisotropy is updated to evaluate the slope stability based on slope geometry and soil properties. Combined with existing research results, the effectiveness of the proposed chart for assessing the slope stability and possible failure mode is verified.

Acknowledgements The authors are grateful to the financial support from the National Natural Science Foundation of China (No. 52078086) and the Program of Distinguished Young Scholars, Natural Science Foundation of Chongqing, China (cstc2020jcyj-jq0087).

Author contribution Li Yongqin: investigation, writing-original draft, visualization. Goh ATC: conceptualization, writing-review and editing. Zhang Runhong: validating, data curation. Zhang Wengang: methodology, supervision, funding acquisition.

Data availability Some or all data, models, or calculation codes that support the findings of this study are available from the corresponding author upon reasonable request (the data in the figures and tables, etc.).

Declarations

Conflict of interest The authors declare no competing interests.

References

Baker R (2003) A second look at Taylor's stability chart. J Geotech Geoenviron Eng 129(12):1102–1108

Bjerrum L (1973) Problems of soil mechanics and construction on soft clays. State-of-the-art report. In Proceedings 8th ICSMFE, Moscow, 111–159

Chen FY, Zhang RH, Wang Y, Liu HL, Bohlke T, Zhang WG (2020a) Probabilistic stability analyses of slope reinforced with piles in spatially variable soils. Int J Approximate Reasoning 122:66–79

Chen LL, Zhang WG, Gao XC (2020b) Design charts for reliability assessment of rock bedding slopes stability against bi-planar sliding: SRLEM and BPNN approaches. Georisk. https://doi.org/10.1080/17499518.2020.1815215

Chen LL, Zhang WG, Zheng Y (2020c) Stability analysis and design charts for over-dip rock slope against bi-planar sliding. Eng Geol 275:105732

Cheng XH (2001) Conversion relationship between two strength indices for effective stress and total stress. J Chongqing Jianzhu Univ 23(2):22–25 (in Chinese)

Conesa S, Mánica M, Gens A, Huang Y (2019) Numerical simulation of the undrained stability of slopes in anisotropic fine-grained soils. Geomech Geoengin 14(1):18–29

Cudny M, Staszewska K (2021) A hyperelastic model for soils with stress-induced and inherent anisotropy. Acta Geotech. https://doi.org/10.1007/s11440-021-01159-z

D'Ignazio M, Länsivaara TT, Jostad HP (2017) Failure in anisotropic sensitive clays: finite element study of Perniö failure test. Can Geotech J 54:1013–1033

Gao XC, Liu HL, Zhang WG, Wang W, Wang ZY (2019) Influences of reservoir water level drawdown on slope stability and reliability analysis. Georisk 13(2):145–153

Ghorbani J, Airey DW, Carter JP, Nazem M (2021) Unsaturated soil dynamics: finite element solution including stress-induced anisotropy. Comput Geotech 133:104062

Ghorbani J, Alrey DW (2021) Modelling stress-induced anisotropy in multi-phase granular soils. Comput Mech 67:497–521

Grimstad G, Andresen L, Jostad HP (2012) NGI-ADP: anisotropic shear strength model for clay. Int J Numer Anal Meth Geomech 36:483–497

Hu LX, Prunier F, Daouadji A (2020) Influence of elastic anisotropy on the mechanical behavior of soils. Eur J Environ Civ Eng. https://doi.org/10.1080/19648189.2020.1841035

Huynh DVK, Jostad HP, Engin HK (2019) Improvement of $N_{T\text{-}bar}$ evaluation in clays using large deformation FE method. Proceedings of the 1st Vietnam Symposium on Advances in Offshore Engineering: Energy and Geotechnics. M.F. Randolph, Dinh Hong Doan, Anh Minh Tang, Man Bui, Van Nguyen Dinh. Springer, Singapore, Chapter 18, pp 137–143

Hwang J, Dewoolkar M, Ko HY (2002) Stability analysis of two-dimensional excavated slopes considering strength anisotropy. Can Geotech J 39:1026–1038

Jostad HP, Fornes H, Thakur V (2014) Effect of strain-softening in design o fills on gently inclined areas with soft sensitive clays. Landslides in Sensitive Clays From Geosciences to Risk Management. Jean-Sébastien L'Heureux, Ariane Locat, Serge Leroueil, Denis Demers, Jacques Locat. Springer, Chapter 24, pp 305–317

Li YQ, Zhang WG (2020) Investigation on passive pile responses subject to adjacent tunnelling in anisotropic clay. Comput Geotech 127:103782

Li YQ, Zhang WG, Zhang RH (2021) Numerical investigation on performance of braced excavation considering soil stress-induced anisotropy. Acta Geotech. https://doi.org/10.1007/S11440-021-01171-3

Lim K, Lyamin AV, Li AK (2016) Three-dimensional slope stability charts for frictional fill materials placed on purely cohesive clay. Int J Geomech 16(2):04015042

Liu H, Feng YZ, Zhang WY, Ji GA (2021) Study on influence of principal stress direction angle on anisotropy of remolded loess. Water Resour and Hydropower Eng 52(3):155–161 (in Chinese)

Liu YD, Yang XQ, Xu L, Lin YK, Gong X (2018) A stability analysis of slope considering strength anisotropy in soils. J Guangdong Univ Technol 35(6):57–62 (in Chinese)

Liu LL, Zhang P, Zhang SH, Li JZ, Huang L, Cheng YM, Wang B (2022) Efficient evaluation of run-out distance of slope failure under excavation. Eng Geol 306:106751

Luo LH, Zhou J, Cai L, Wen XG (2019) Layered slope stability analysis considering anisotropy. J Cent South Univ 50(8):1884–1890 (in Chinese)

Ning S, Zhuang Y, Tan YZ, Wang DX (2021) Stability analysis of anti-slide pile slope considering soil anisotropy. J China Three Gorges Univ 43(1):43–47

Panagoulias S, Brinkgreve RBJ, Zampich L (2018) PLAXIS MoDeTo manual. Plaxis bv, Delft, The Netherlands

Rao PP, Zhao LX, Chen QS, Nimbalkar S (2019) Three-dimensional limit analysis of slopes reinforced with piles in soils exhibiting heterogeneity and anisotropy in cohesion. Soil Dyn Earthq Eng 121:194–199

Sahoo PP, Shukla SK (2019) Taylor's slope stability chart for combined effects of horizontal and vertical seismic coefficients. Geotechnique 69:344–354

Sahoo PP, Shukla SK, Ganesh R (2020) Taylor's slope stability chart for combined effects of horizontal and vertical seismic coefficients. Geotechnique 70:835–838

Steward T, Sivakugan N, Shukla SK, Das BM (2011) Taylor's slope stability charts revisited. Int J Geomech 11(4):348–352

Stockton E, Leshchinsky BA, Olsen MJ, Evans TM (2019) Influence of both anisotropic friction and cohesion on the formation of tension cracks and stability of slopes. Eng Geol 249:31–44

Tang HX, Wei WC (2019) Finite element analysis of slope stability by coupling of strength anisotropy and strain softening of soil. Rock and Soil Mechanics 40(10):4092–4100 (in Chinese)

Tang HX, Wei WC, Liu F, Chen GQ (2020) Elastoplastic Cosserat continuum model considering strength anisotropy and its application to the analysis of slope stability. Comput Geotech 117:103235

Taylor DW (1937) Sability of earth slopes. J Boston Soc Civ Eng 24:197–246

Tu YL, Liu XR, Zhong ZL, Li YR (2016) New criteria for defining slope failure using the strength reduction method. Eng Geol 212:63–71

Ukritchon B, Boonyatee T (2015) Soil parameter optimization of the NGI-ADP constitutive model for Bangkok soft clay. Geotech Eng 46:28–36

Verreydt K, Van Gemert D, Rauwoens P, Houtmeyers J, Claes T (2019) Analysis of a full-scale slope failure test on a sludge embankment. Proceedings of the Institution of Civil Eng – Geotech Eng 172(5):417–431

Xia YY, Chen CS (2018) Seismic stability limit analysis of reinforced soil slopes with prestressed cables considering inhomogeneity and anisotropy of multiple parameters. Chin J Rock Mech Eng 37(4):830–838

Xu P, Sun ZJ, Shao SY (2021) Strength characteristics based on variation of spatial mobilization plane for anisotropic geomaterials. Chinese J Geotech Engi 43(6):118–1124

Yeh P, Lee KZ, Chang K (2020) 3D Effects of permeability and strength anisotropy on the stability of weakly cemented rock slopes subjected to rainfall infiltration. Eng Geol 266:105459

Yuan W, Li JX, Li ZH, Wang W, Sun XY (2020) A strength reduction method based on the Generalized Hoek-Brown (GHB) criterion for rock slope stability analysis. Comput Geotech 117:103240

Zapata-Medina DG, Cortes-Garcia LD, Finno RJ, Arboleda-Monsalve LG (2020) Stiffness and strength anisotropy of overconsolidated bootlegger cove clays. Can Geotech J 57(7):1652–1663

Zhang RH, Wu CZ, Goh ATC, Bohlke T, Zhang WG (2020) Estimation of diaphragm wall deflections for deep braced excavation in anisotropic clays using ensemble learning. Geosci Front. https://doi.org/10.1016/j.gsf.2020.03.003